

Microseismicity linked to gas migration and leakage on the western Svalbard shelf

Peter Franek¹, Andreia Plaza-Faverola¹, Jürgen Mienert¹, Stefan Buenz¹, Bénédicte Ferré¹, Alun Hubbard¹

¹CAGE – Centre for Arctic Gas Hydrate, Environment and Climate, Department of Geosciences, UiT The Arctic University of Norway, Postboks 6050 Langnes, N-9037 Tromsø, Norway

Contents of this file

Text S1
Figures S1 to S7
Table S1

Additional Supporting Information (Files uploaded separately)

Caption for Table S1

Introduction

This supporting information provides earthquake catalogue of known earthquakes that occurred during the 10 month operational period of the MASOX observatory with epicenters within the domain bounded from 25°W to 40°E and 70°N to 90°N (Table S1). It also provides supplementing information on determining orientation of horizontal components of the OBS relative to the geographical north through polarization analysis of earthquake generated P-waves (Text S1, Figure S1). Supplementary Figure S2 illustrates variability of particle motion of earthquake generated P-waves used in the polarization analysis. Supplementary Figure S3 shows particle motion of representative SDEs. Supplementary Figure S4 and S5 accompany time series analysis of the SDE occurrence and bottom water temperature presented in the main text. Supplementary Figure S6 and S7 illustrate similarity between the HF-SDEs and published records of "20 Hz" finback whale calls.

Text S1.

To determine seismometer orientation with respect to the geographic north an arbitrarily chosen horizontal component of non-oriented OBS horizontals can be considered temporarily as north component and the other horizontal as east component of the seismometer. We opt component H2 and H1 for the north and the east, respectively. Seismometer orientation is then determined using this frame of reference. Considering clockwise measured angles as positive, the seismometer orientation using earthquake generated P-wave record is determined in these steps:

1. For known epicenter of the earthquake a station-to-earthquake azimuth φ is determined. This angle is measured from the geographic north.
2. An apparent back-azimuth α is determined using horizontal particle motion of the earthquake's P-wave. This angle is measured from temporarily chosen north component of the seismometer, i.e., from the component H2.
3. Apparent back-azimuth α determined in previous step is ambiguous with 180° modulo since the P-wave particle motion can be oriented towards or away from the source (see Figure S1). The first motion of P-wave on the vertical component Z enables to completely resolve this ambiguity – downward first motion means horizontal motion towards the source and upward first motion means horizontal motion outwards from the source. Using this approach the apparent back-azimuths of earthquakes are unambiguously determined and 180° uncertainty is eliminated.
4. Finally, the seismometer orientation ϑ with respect to the geographic north is calculated using $\vartheta = \alpha - \varphi$.

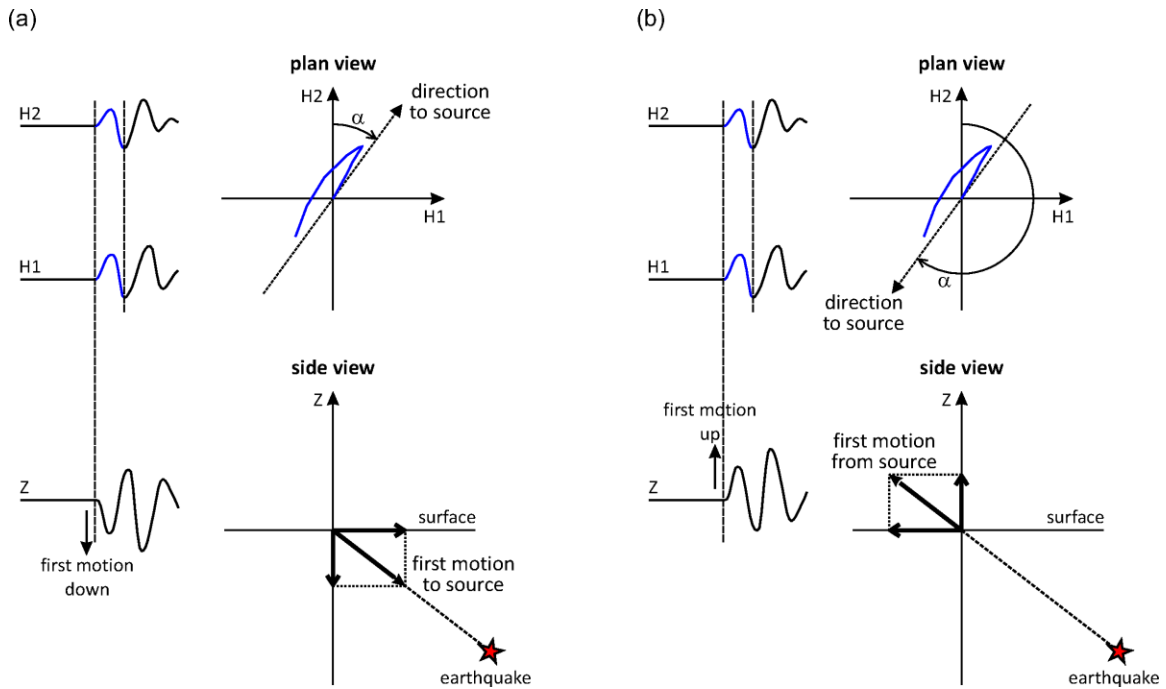


Figure S1. Example illustrating polarization analysis of earthquake generated P-wave. Horizontal motion is used to determine the apparent back-azimuth, i.e., an angle of impinging seismic wave measured clockwise from the component H2. This motion can be oriented (a) towards the source or (b) outward from the source. Polarity of the P-wave's first motion in the vertical component Z is used in order to identify correct back-azimuth.

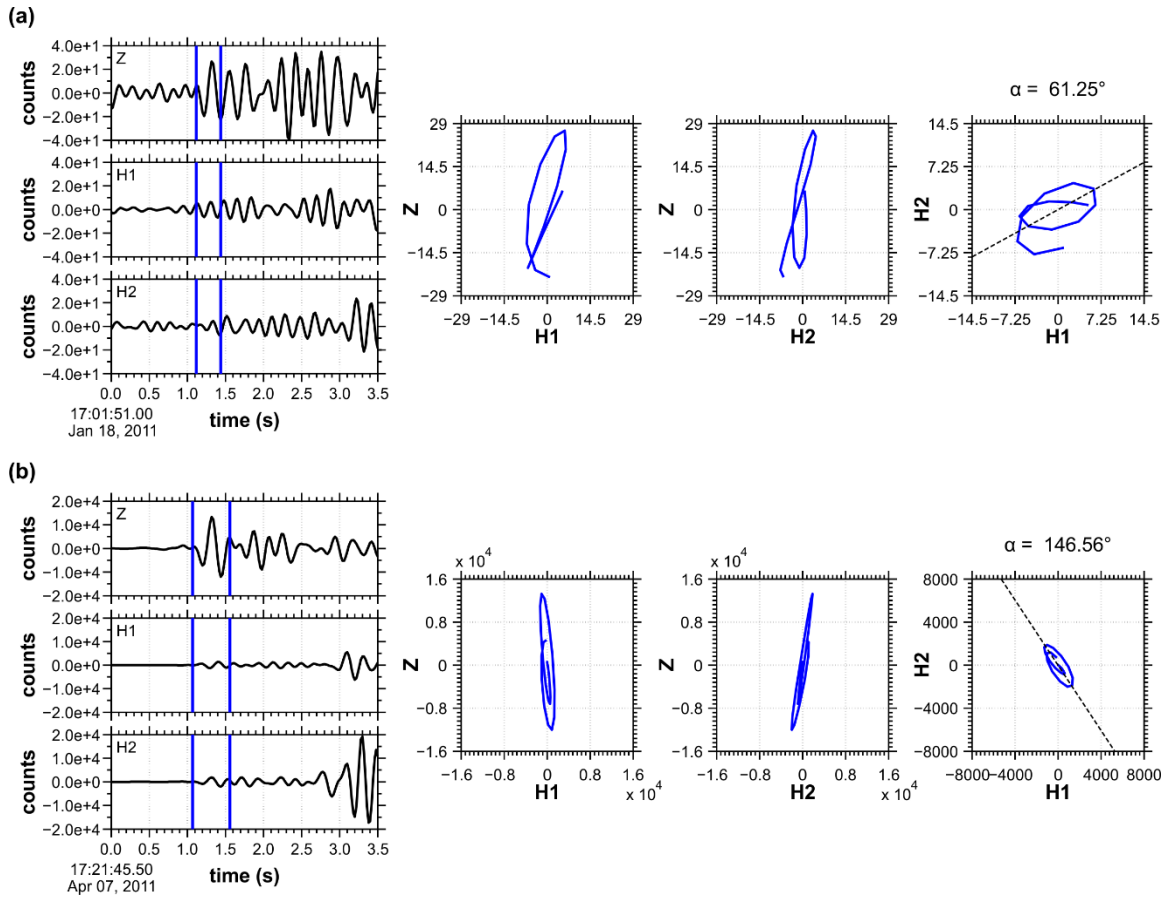


Figure S2. Left side: Filtered seismic records (2-6 Hz band-pass Butterworth filter) with P-wave of (a) an earthquake with magnitude $M=3.2$ at an epicenter distance ~ 276 km (earthquake no. 86 in Table S1) and (b) an earthquake with magnitude $M=3.6$ at an epicenter distance ~ 32 km (earthquake no. 183 in Table S1; Figure 3). Blue lines indicate part of the records that was used to determine the orientation of seismometer with respect to the geographic north. Right side: Particle motion of the selected part of earthquakes generated P-wave illustrating (a) less confined wave onset and polarization due to the presence of noise signals and (b) well-defined onset and polarization. The particle motion is shown in two vertical planes (H1 versus Z component, H2 versus Z component) and in the horizontal plane (H1 versus H2 component). α is apparent back-azimuth determined from the horizontal motion.

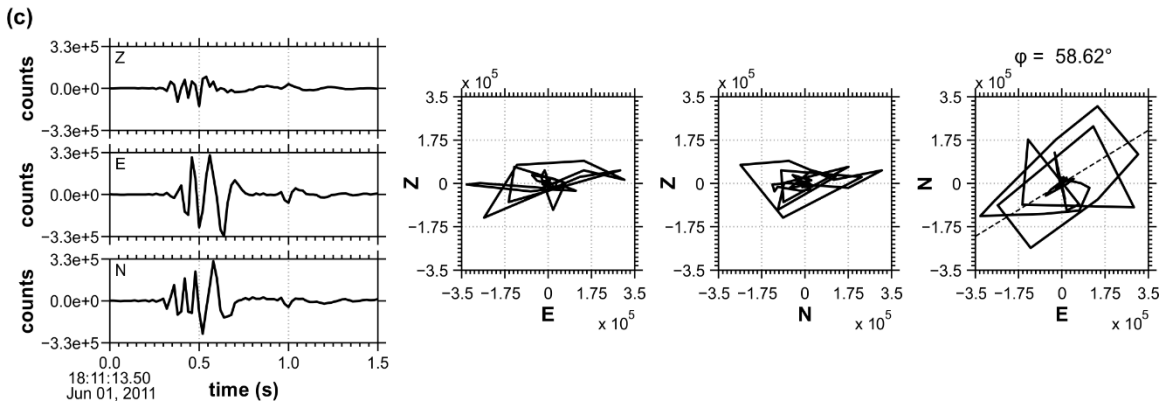
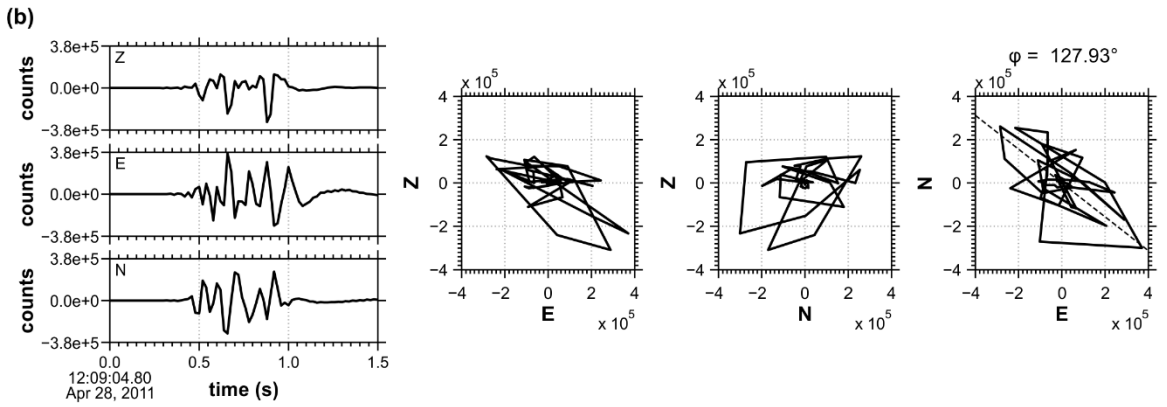
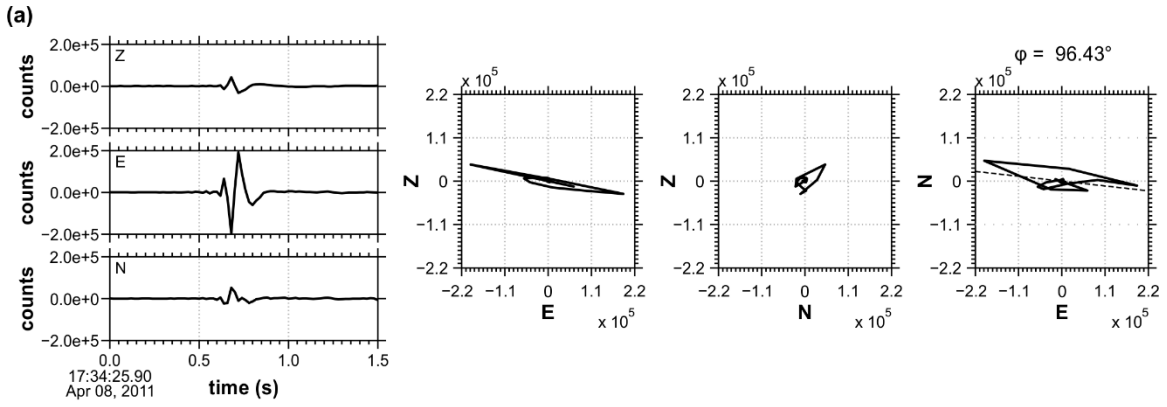


Figure continues on the next page.

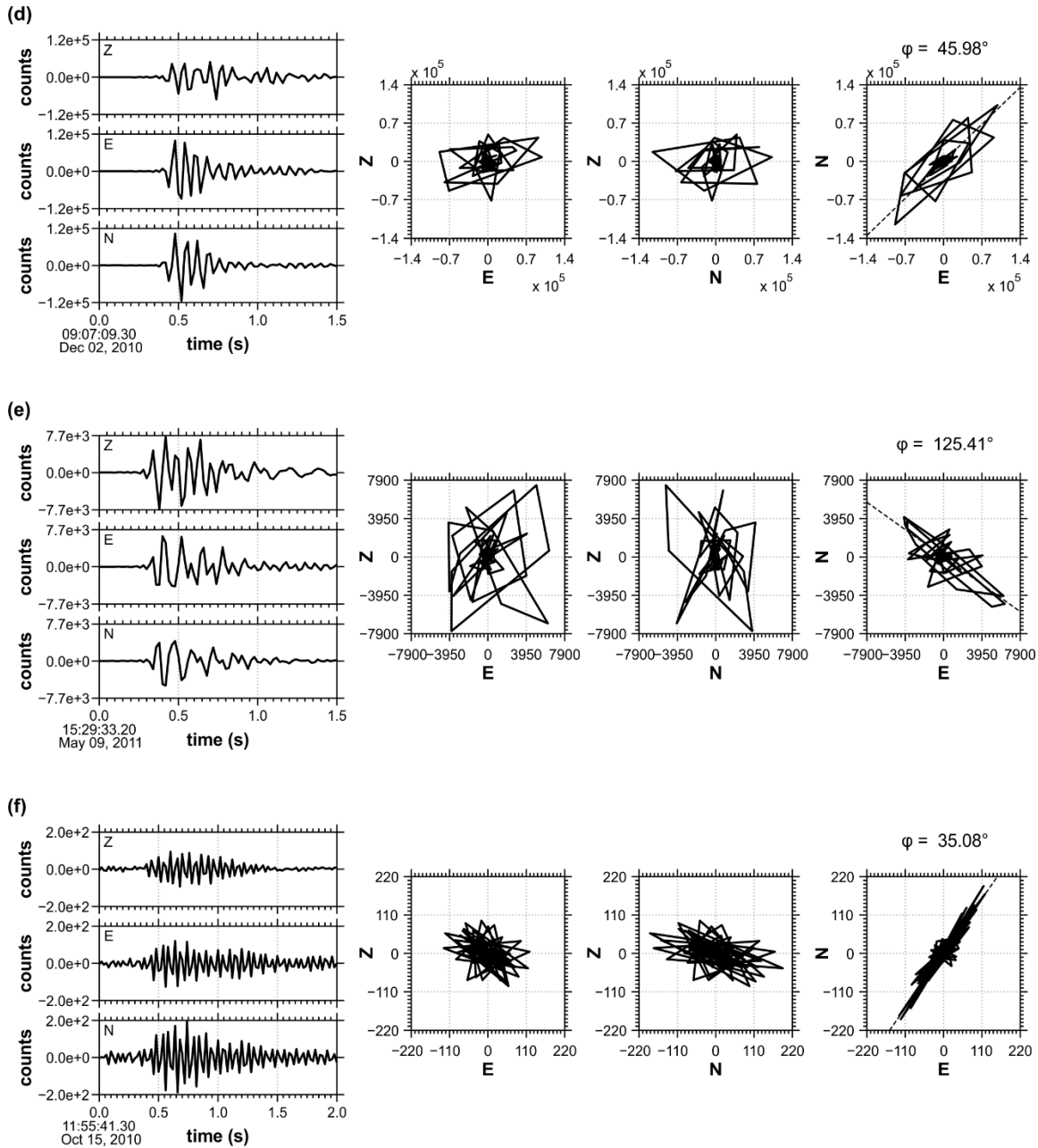


Figure S3. (a-f) Left side: 3-component seismic records (1.5-24 Hz band-pass Butterworth filter) of the SDEs shown in Figure 6. Right side: Particle motion of corresponding seismograms shown in two vertical planes (E versus Z component, N versus Z component) and in a horizontal plane (E versus N component). ϕ is back-azimuth determined from the horizontal motion.

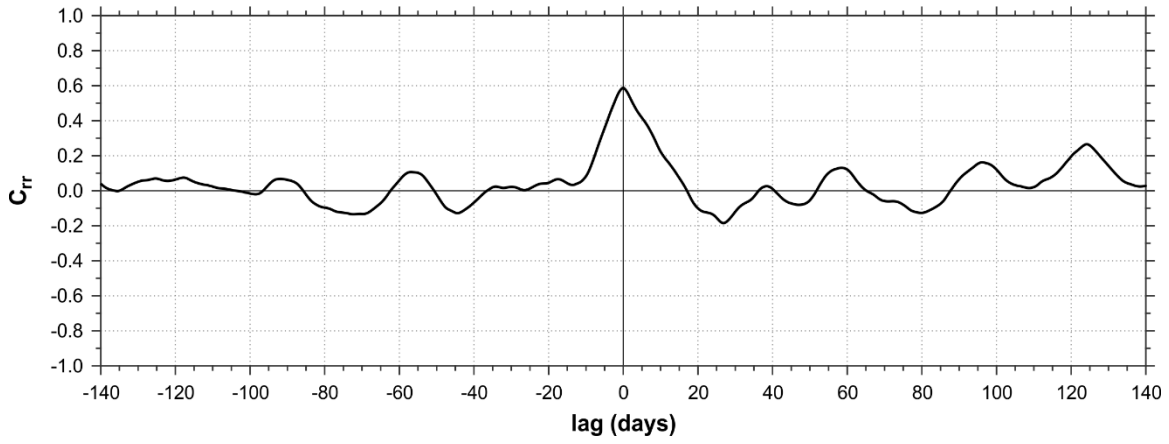


Figure S4. Cross-correlation between residuals in the daily occurrence of SDEs and bottom water temperature after removing fitting functions from smoothed distributions (Figure 10c) demonstrating strong coupling of these two time series at zero lag time.

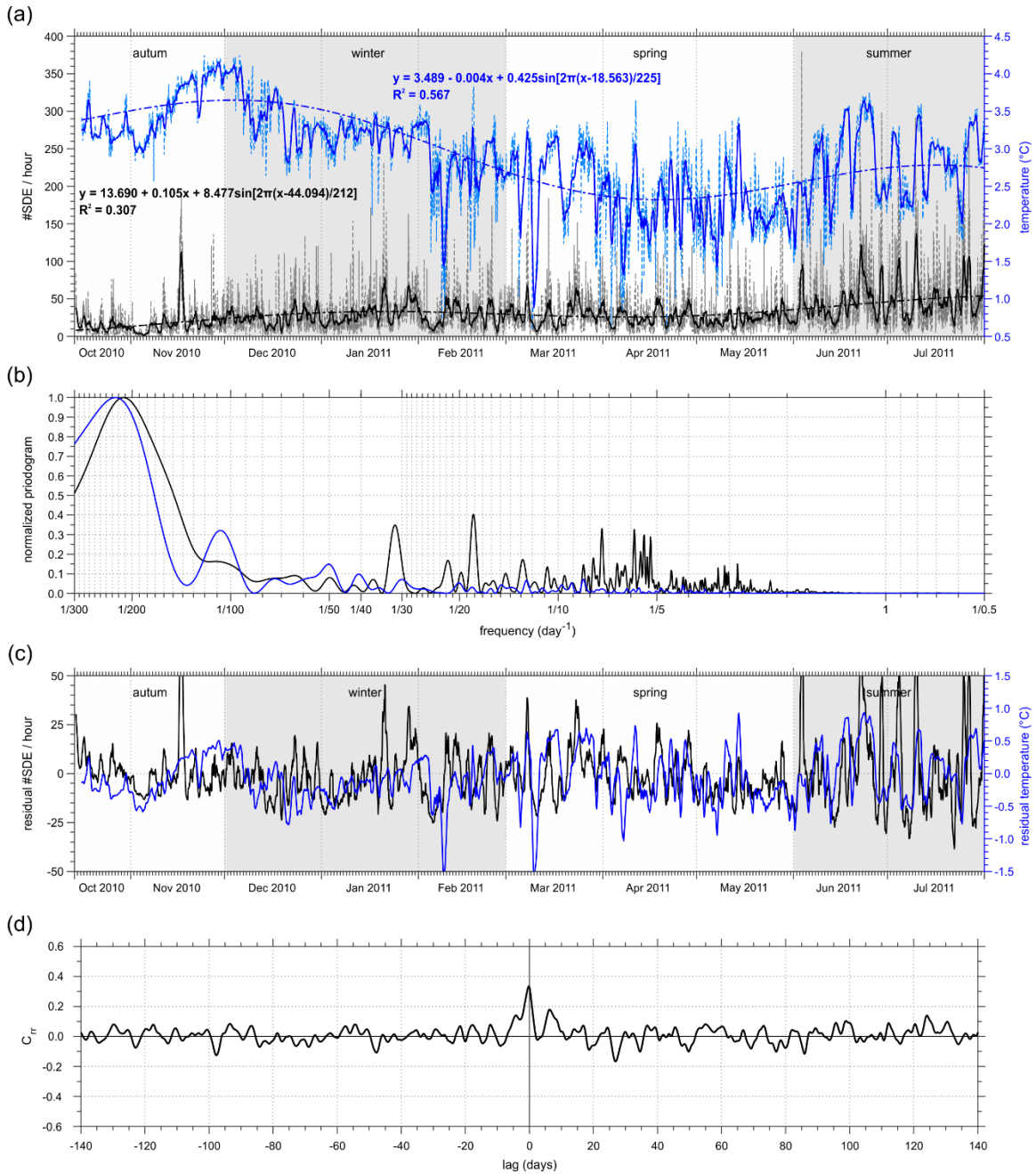


Figure S5. (a) Hourly occurrence of the SDEs during the whole operational period of the OBS deployment (black dashed line) and bottom water temperature recorded at the MASOX location (blue dashed line) [Berndt et al., 2014]. Patterns in both distributions are highlighted by applying a 24 hour moving average filter (solid lines). Dash-dotted lines are least-square fits to the smoothed distributions with fitting functions consisting of linear and sinusoidal parts, for which periods of 212 and 225 days determined from periodograms were imposed. (b) Normalized Lomb-Scargle periodograms determined for smoothed hourly occurrence of the SDEs and bottom water temperature after de-trending by linear regression. (c) Residuals in hourly occurrence of the SDEs and bottom water temperature after removing fitting functions from smoothed distributions. (d) Cross-correlation between residuals demonstrating coupling

of these two time series at zero lag time. Smaller coupling than cross-correlation shown in Figure S4 is due to the use of hourly occurrence of the SDEs and smoothing by 24 hour moving average filter resulting in less effective suppressing of fine-scale variations in the data.

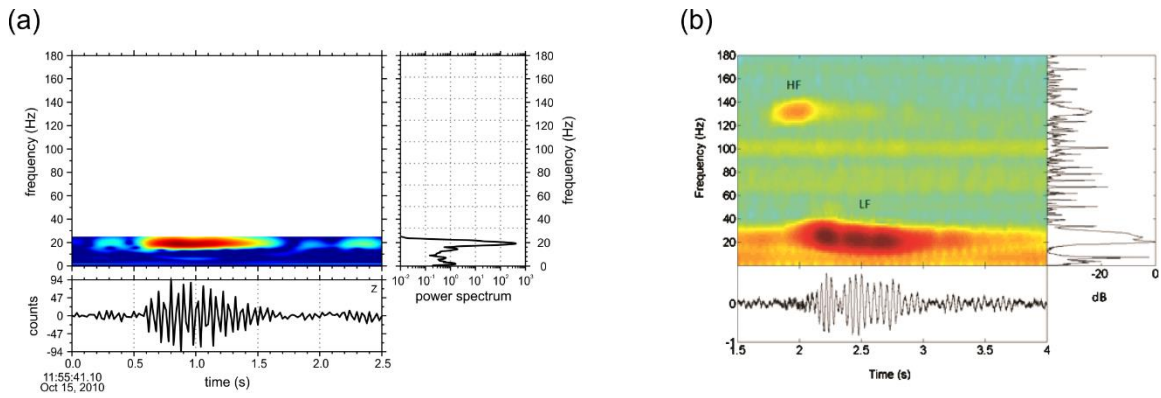


Figure S6. Vertical component Z of seismic record showing waveform of the HF-SDE from Figure 6f, its spectrogram and power spectrum. 25 Hz upper limit of the spectrogram and power spectrum is due to sampling rate (20 ms) of the OBS. (b) An example of waveform, spectrogram and power spectrum of acoustic record of typical finback whale call (Figure 3 from Simon et al. [2010]).

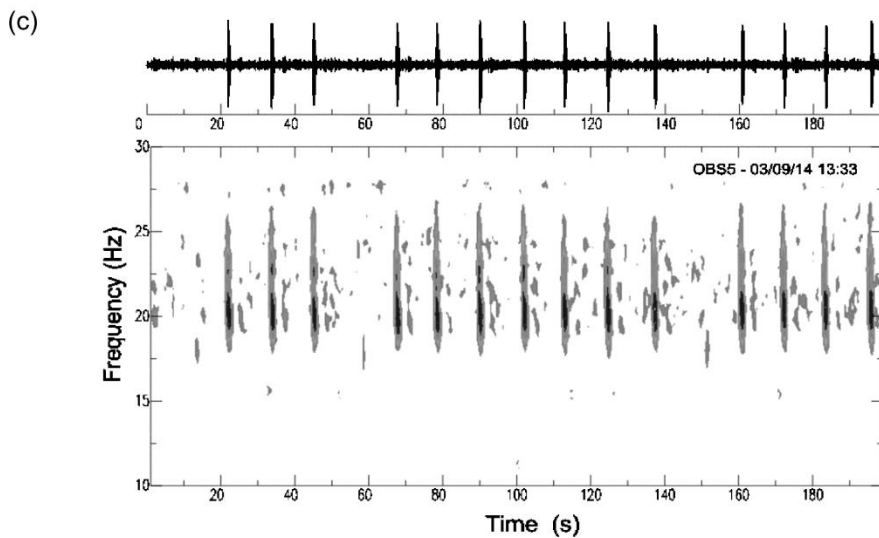
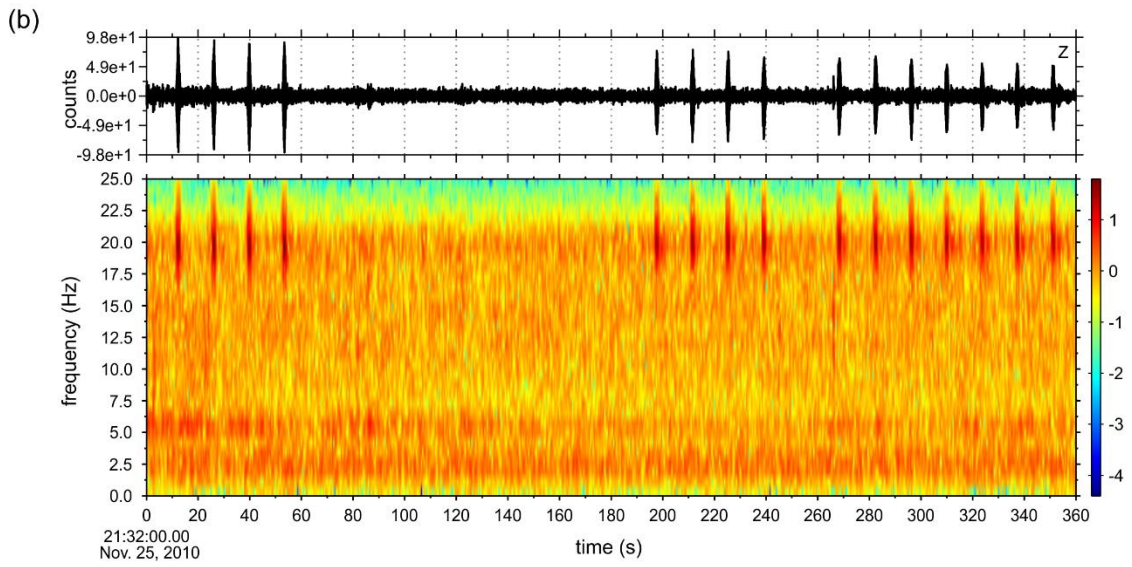
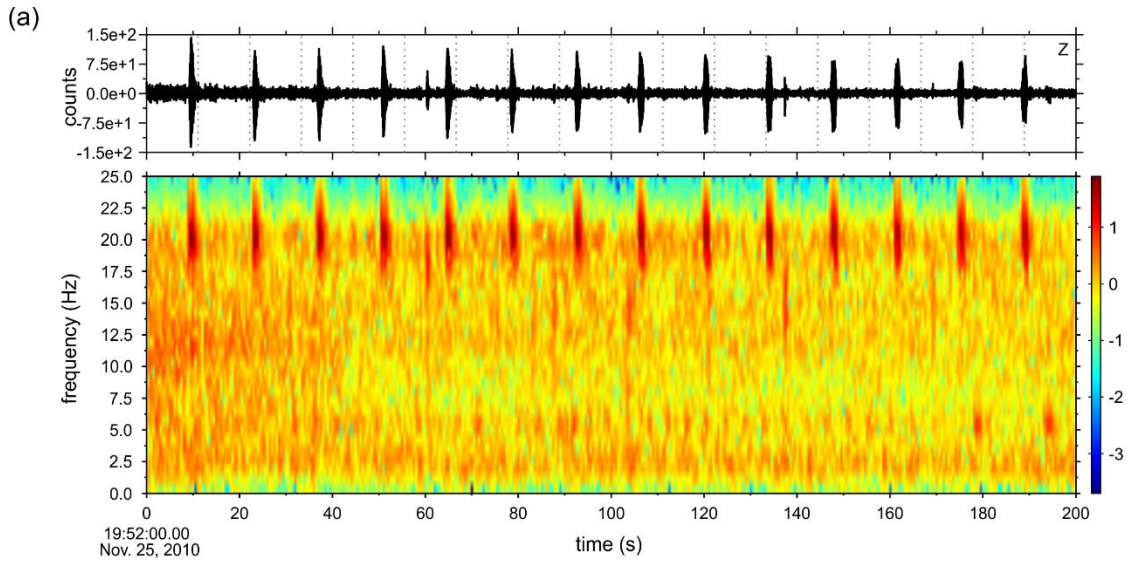


Figure S7. (a-b) Two examples of vertical records Z and their spectrograms (frame length 1.0 s, 50% overlap, Tukey window with 0.5 s total length of tapered section) showing repeatedly occurring HF-SDEs at ~20 Hz. Note no occurrence of events between 60 – 200 s in (b) that may be associated with whale surfacing and breathing. (c) For comparison is shown OBS record with spectrogram of "20 Hz" calling sequence of a finback whale (Figure 3 from Rebull et al. [2006]).

Table S1. Earthquake catalogue extracted from the Reviewed Bulletin of the International Seismic Center (<http://www.isc.ac.uk>) and from the NORSAR regional reviewed bulletin (<http://www.norsardata.no/NDC/bulletins/regional>).